$^{11}B+^{12}C$ and $^{10}B+^{13}C$ fusion cross sections

J. F. Mateja
Physics Department, Tennessee Technological University, Cookeville, Tennessee 38501

A. D. Frawley, L. C. Dennis, K. Abdo, and K. W. Kemper
Physics Department, Florida State University, Tallahassee, Florida 32304

(Received 13 November 1981)

Heavy particle residues arising from the $^{11}B+^{12}C$ and the $^{10}B+^{13}C$ entrance channels have been mass identified with a time-of-flight system for boron projectile energies from 14 to 54 MeV in one MeV intervals. Both entrance channels cover a ^{23}Na excitation energy range from approximately 25 to 50 MeV. With the exception of decays to the mass 15 and 18 residues, the decay of the $^{11}B+^{12}C$ system to a particular mass is similar in magnitude and energy dependence to the decay of the $^{10}B+^{13}C$ system to that mass. This similarity in the two systems and the differences in the mass 15 and 18 decays can be explained in terms of the entrance channel angular momenta and the available decay channels. In addition to the individual decay cross sections, the total $^{11}B+^{12}C$ and $^{10}B+^{13}C$ fusion cross sections have been measured. Both entrance channels show evidence of a fusion cross section limitation. These limitations cannot presently be explained in terms of a critical compound nucleus level density.

[NUCLEAR REACTIONS $^{12}C(^{11}B,X)$, $14 \leq E_{lab} \leq 54$ MeV; $^{12}C(^{11}B,^{11}B)^{12}C$, $E_{lab}=25$, 40, and 50 MeV; $^{13}C(^{10}B,X)$, $14 \leq E_{lab} \leq 48$ MeV; $^{13}C(^{10}B,^{10}B)^{13}C$, $E_{lab}=18$, 25, 32, 39, and 46 MeV; measured $d^2\sigma/d\Omega\, dE$ for reaction products $M=9-22$; deduced critical and grazing angular momenta.]

I. INTRODUCTION

The causes of the limitation in the fusion cross section for heavy-ion systems in the $1p$ and $2s$-$1d$ subshells have been an outstanding problem for a number of years. Macroscopic models were first used to explain the fusion cross section limitations observed between different systems and the subsequent variations in the maximum fusion cross section which were observed in going from one system to another. The macroscopic models, like those of Bass,[1] Horn and Ferguson,[2] and Krappe and Nix,[3] based the dependence of the fusion cross sections on quantities such as the mean nuclear density and the mean nuclear potential. However, substantial discrepancies between the model predictions and experimental fusion cross sections have been reported in an extensive study of fusion cross sections in this mass region.[4]

More recent experimental work has suggested that the fusion cross sections may depend on either the microscopic nature of the entrance channel nuclei[4,5] or on the characteristics of the compound nucleus formed.[6–8]. Strong variations in the maximum fusion cross sections from one entrance channel to another (sometimes differing by only a single nucleon) have been used as evidence to support the microscopic interaction argument.[4,5] On the other hand, in those cases where two different entrance channels leading to the same compound nucleus have been studied, the two entrance channels have been observed to reach the same critical angular momentum at the same compound nucleus excitation energy.[6–8] This angular momentum limitation has been attributed to either the position of the compound nucleus yrast line[6] or to some critical density of compound nucleus states having been reached.[7–9]

In an earlier paper[10] we reported the total fusion cross sections for two entrance channels which formed the ^{23}Na compound nucleus, $^{11}B+^{12}C$ and $^{10}B+^{13}C$. From these total fusion cross sections, it was apparent that the limitation in the fusion cross section for these two systems was not due to a property of the compound nucleus since the two entrance channels do not reach the same critical angular momentum at the same compound nucleus excitation energy. In the present paper, the fusion cross

sections to the individual residual mass groups for these two systems are studied in an attempt to obtain further insights into this problem.

II. EXPERIMENTAL PROCEDURES AND RESULTS

Beams of ^{11}B and ^{10}B were produced by the Florida State University (FSU) inverted sputter source and then accelerated over a laboratory energy range from approximately 14 to 54 MeV by the FSU super FN tandem Van de Graaff accelerator. These beams were used to bombard self-supporting ^{12}C or ^{13}C targets whose nominal thicknesses ranged from 70 to 100 $\mu g/cm^2$. Carbon buildup during the runs was minimized by surrounding the target with a liquid nitrogen cooled shroud. Carbon buildup was found to be about 4% over the duration of one excitation function. The principal contaminant in the ^{12}C target was found to be ^{16}O (2%), while the ^{13}C targets contained small amounts of ^{12}C (3%) and ^{16}O (2%).

The evaporation residues resulting from the complete fusion of the target and projectile were mass identified with a time-of-flight system, shown schematically in Fig. 1. A microchannel plate detector marked the initial passage of the heavy residues which were then stopped in a silicon surface barrier detector 2.7 m downstream. The typical time resolution of ≈ 500 psec, obtained for both experiments, was sufficient to produce unit mass resolution over the entire bombarding energy range. The present experimental arrangement is well suited for accurate identification of particles with energies as low as 2 or 3 MeV. Monitors positioned to the left and right of the beam allowed for an accurate determination of the beam position.

A two-dimensional time versus energy spectrum was recorded on line at each energy and angle. Conversion from a time to a mass scale was made later. A contour plot of one such mass versus energy spectrum is shown in Fig. 2.

Angular distributions of the evaporation residues were measured from 3° to 40° in the laboratory to obtain the total fusion yield. Because the shapes of the angular distributions change slowly as a function of energy (see Fig. 3), it was only necessary to measure complete angular distributions at energy intervals of several MeV (5 MeV for $^{11}B+^{12}C$ and 7 MeV for $^{10}B+^{13}C$). The measured angular distributions were then used to obtain the total fusion cross section from the single angle yields of an excitation function measured in one MeV steps (8° for $^{11}B+^{12}C$ and 9° for $^{10}B+^{13}C$).

In evaluating the total fusion cross section for either system, the energy spectra of all exit channel mass groups were inspected for evidence of nonfusion events (i.e., direct transfer, inelastic scattering, and knockout) before that mass was included in the calculation of the total fusion cross section. Events which formed discrete peaks in the energy spectrum of a particular exit channel were considered to be nonfusion. In general, such direct transfer or inelastic scattering events have energies near that of the projectile. In addition, to further discriminate between fusion and nonfusion events, each exit channel energy spectrum for the $^{11}B+^{12}C$ entrance channel was compared with its corresponding exit channel for the $^{10}B+^{13}C$ entrance

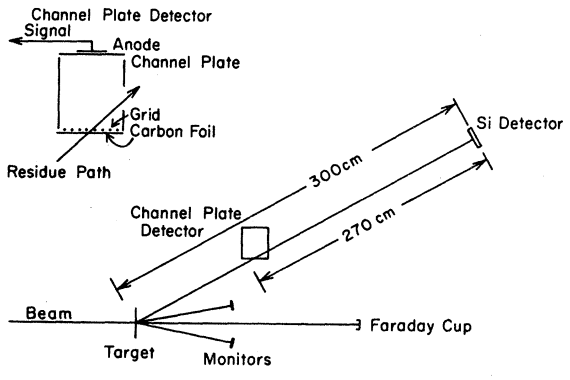

FIG. 1. Schematic of the time-of-flight system.

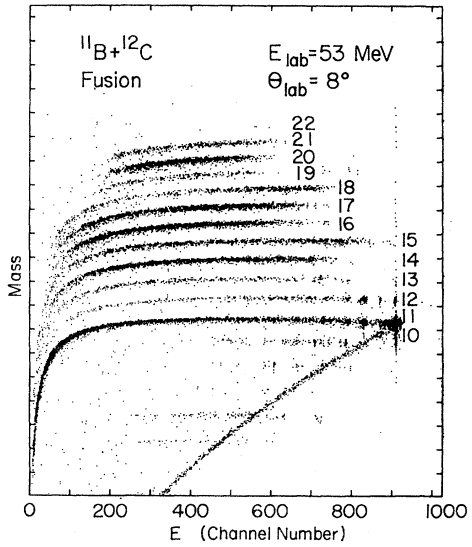

FIG. 2. A representative mass versus energy contour map for the $^{12}C+^{11}B$ system.

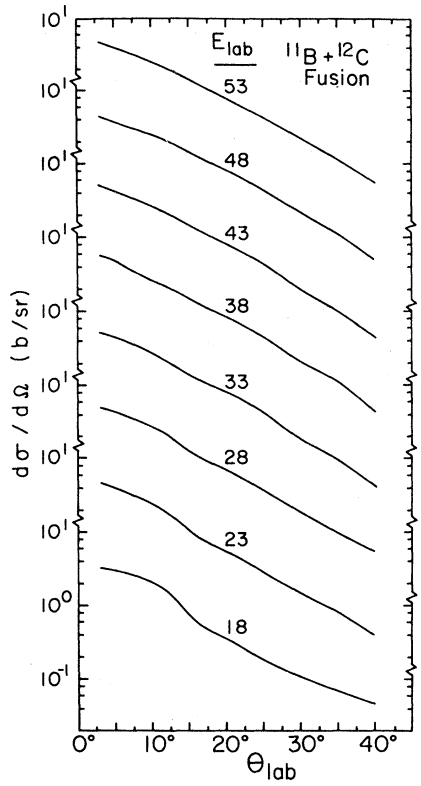

FIG. 3. Angular distributions of the evaporation residues for the $^{12}C+^{11}B$ system.

channel. If the comparison is made at the same compound nucleus excitation energy, the shapes of the fusion evaporation residue energy distributions should be similar. The presence of a direct component in one system should cause a readily apparent difference between the residual-mass energy spectra for the two entrance channels.

Under the above conditions, no evidence of nonfusion events was found for either entrance channel for decay masses from 14 to 22. For masses ≤ 13, however, both entrance channel systems exhibited discrete peaks at energies near the projectile energy. These peaks were most evident at the highest bombarding energies. This yield was assumed to arise from either direct transfer or inelastic scattering and was not included in the fusion yield for that mass. Had the total nonfusion yield to all masses ≤ 13 been included, the total fusion cross section would have been increased by less than 5% in each experiment.

An additional complication arose in the elastic scattering exit channel for both systems. The mass 10 and mass 11 fusion cross sections were obscured in the $^{10}B+^{13}C$ and $^{11}B+^{12}C$ experiments, respectively, due to the backgrounds from inelastic scattering. However, the fusion yield to the mass 10 group could be measured in the $^{11}B+^{12}C$ study and was found to be $\leq 1\%$ of the total fusion cross section at all energies. We have, therefore, excluded the mass 10 yield when evaluating the total fusion cross sections for both systems. The mass 11 yield could be evaluated in the $^{10}B+^{13}C$ study. This cross section was found to vary smoothly from zero to $\simeq 60$ mb over the energy range investigated. This cross section has been included in the $^{10}B+^{13}C$ total fusion cross section but has been excluded from the $^{11}B+^{12}C$ total fusion cross section since a reliable mass 11 fusion cross section could not be obtained.

Finally, as can be seen in Fig. 2, the heavy products with masses <10 showed no events which could be attributed to fusion at any of the bombarding energies studied in this experiment. The excitation functions for the evaporation residues arising from the fusion of $^{11}B+^{12}C$ and $^{10}B+^{13}C$ are presented in Fig. 4. The total fusion cross sections for these two systems are presented in Fig. 5.

The absolute cross sections were determined in both the $^{11}B+^{12}C$ and the $^{10}B+^{13}C$ experiments by measuring the product of the target thickness and detector solid angle ($N_T\Omega$). Twenty MeV ^{16}O ions were elastically scattered from both the ^{12}C and ^{13}C targets. At angles of 15° and 20° the scattering of ^{16}O is Rutherford scattering. These results were then compared to the $N_T\Omega$ values obtained from the forward angle (8°—20°), low energy (14 to 18 MeV) ^{10}B elastic scattering yields, which were measured simultaneously with the fusion yields. At these energies and angles the ^{10}B elastic scattering cross sections were found to be equal to the Rutherford scattering cross section. The two estimates of the $N_T\Omega$ values agreed to within 4%.

The uncertainties in the total fusion cross sections are attributable to counting statistics ($\leq 2.5\%$), angle setting uncertainties (4%), identification of fusion products (3%), extrapolation of the data to zero degrees and beyond 40° (4%), the normalization of the single-angle excitation functions to the angular distribution (3%), and errors in measuring the absolute target thickness ($\approx 6\%$). The total uncertainty in the absolute cross sections is therefore approximately 10%. However, since the same experimental system and techniques were used to measure both the $^{11}B+^{12}C$ and the $^{10}B+^{13}C$ fusion cross sections, we believe that the relative error between the two systems is likely to be somewhat smaller.

In addition to the fusion cross sections, elastic

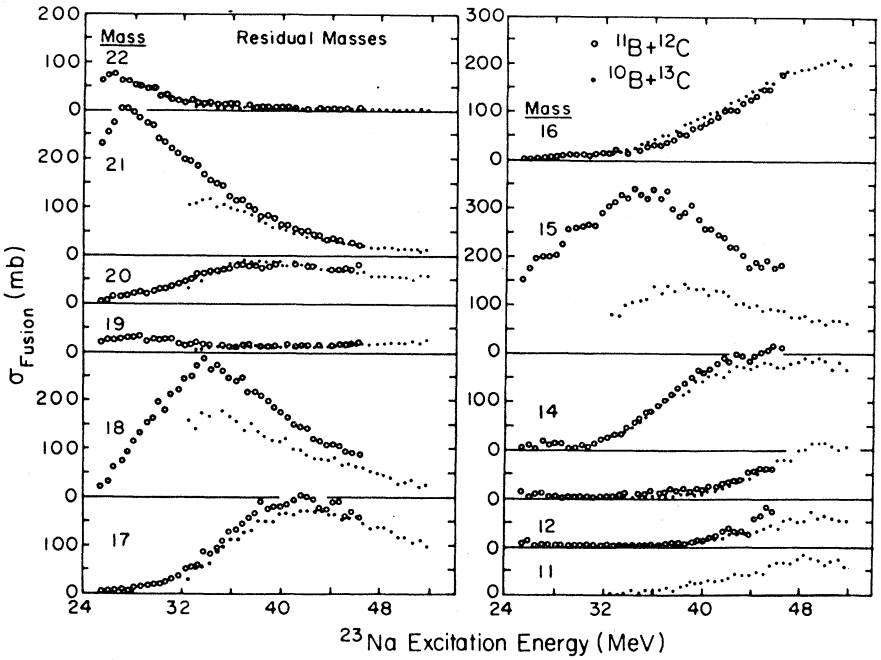

FIG. 4. Angle-integrated yields for evaporation residues from the $^{11}B+^{12}C$ and $^{10}B+^{13}C$ systems over a ^{23}Na excitation energy range from approximately 24 to 50 MeV.

scattering cross sections were measured for both entrance channels. For the $^{10}B+^{13}C$ experiment, the elastic scattering data, displayed in Fig. 6, were obtained simultaneously with the fusion yield. However, because of known single particle exchange effects,[11] more detailed elastic scattering angular distributions were measured for the $^{11}B+^{12}C$ system. These angular distributions, measured at energies of 25, 40, and 50 MeV, are presented in Fig. 7. The previously reported elastic transfer cross section[11] is clearly evident beyond an angle of 70°, where the cross section begins to rise sharply.

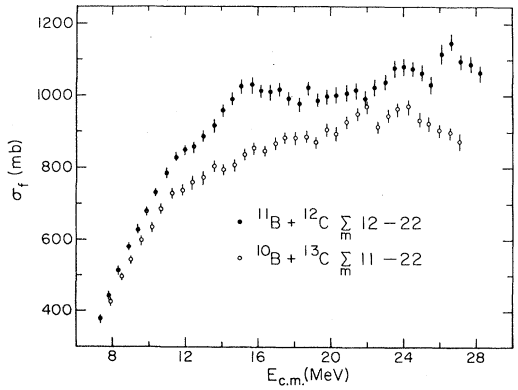

FIG. 5. Total fusion cross section excitation functions for the $^{11}B+^{12}C$ and $^{10}B+^{13}C$ systems. Included in the $^{11}B+^{12}C$ total fusion cross section are evaporation residues with masses from 12 to 22, while masses from 11 to 22 have been included in the $^{10}B+^{13}C$ total fusion cross section.

III. OPTICAL MODEL ANALYSIS

Optical model analyses of the $^{10}B+^{13}C$ and $^{11}B+^{12}C$ elastic scattering data were performed to determine the energy dependence of the total reaction cross sections and the grazing angular momenta for these systems. The optical model parametrization of the elastic scattering data, performed with the computer code JIB,[12] employed a Woods-Saxon potential of the form

$$U(r)=-V_0 f(r)-iW_0 f(r)+V_c(r)\ ,$$

where

$$f(r)=1/[1+\exp(r-R_r/a_r)]\ ,$$

$$V_c(r)=\frac{z_1 z_2 e^2}{2R_c}(3-r^2/R_c^2),\quad r\le R_c$$

$$=\frac{z_1 z_2 e^2}{r}\ ,\quad r>R_c\ ,$$

and

$$R_{r,i,c}=r_{r,i,c}(A_t^{1/3}+A_p^{1/3})\ .$$

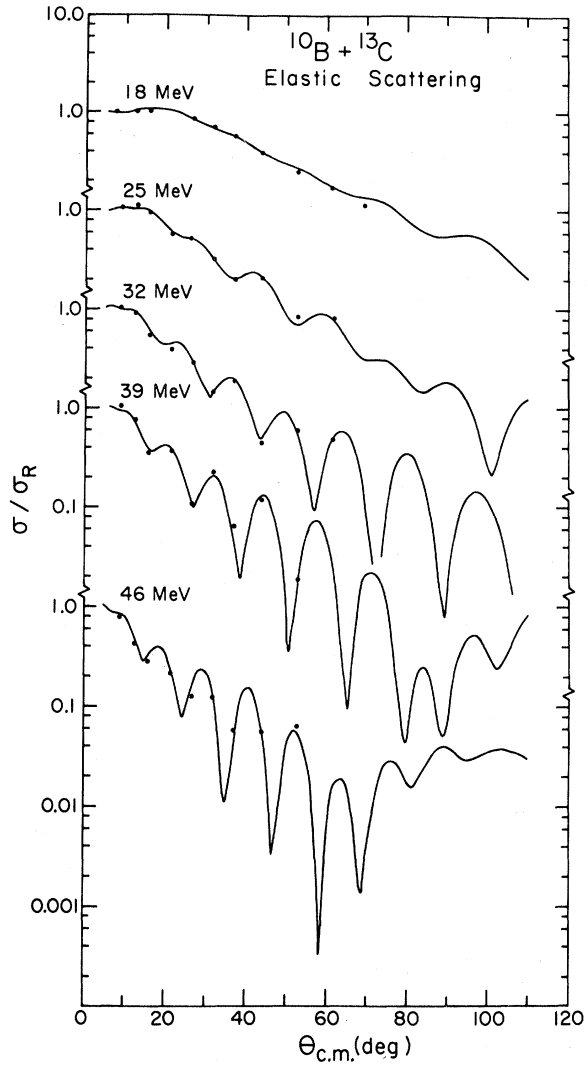

FIG. 6. $^{10}B+^{13}C$ elastic scattering angular distributions. The solid curves represent optical model fits to the data obtained with an energy independent optical model parameter set.

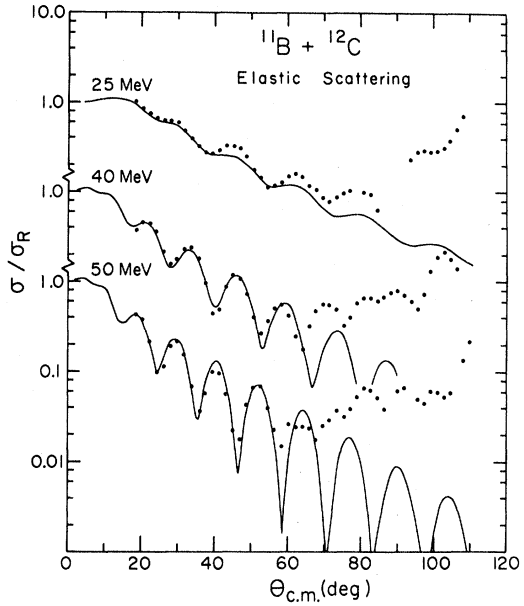

FIG. 7. $^{11}B+^{12}C$ elastic scattering angular distributions. The solid curves represent optical model fits to the forward angle data obtained with an energy independent optical model parameter set. The increase in the back angle cross section is believed to be due to exchange effects. Consequently, no effort was made to fit this region.

Details of the procedure used to extract optical model parameters from elastic scattering data have been outlined elsewhere.[13] An energy independent set of optical model parameters was found to fit each elastic scattering system. The results of the fits to the $^{10}B+^{13}C$ and the $^{11}B+^{12}C$ data are presented in Figs. 6 and 7, respectively, and the optical model parameters are listed in Table I. It should be noted that only $^{11}B+^{12}C$ data out to $\approx 60°$ were used in the fitting procedure, due to the importance of the elastic transfer cross section beyond this angle.

TABLE I. Optical model parameters for the elastic scattering of ^{11}B from ^{12}C and ^{10}B from ^{13}C. Parameter sets *B* and *C* for the $^{11}B+^{12}C$ system were taken from Refs. 14 and 15, respectively.

System		V_0 (MeV)	r_r (fm)	a_r (fm)	W_0 (MeV)	r_i (fm)	a_i (fm)	r_c (fm)
$^{10}B+^{13}C$		66.85	1.094	0.609	10.00	1.200	0.700	1.250
$^{11}B+^{12}C$								
	A	60.50	1.094	0.609	36.04	1.182	0.487	1.300
	B	100.00	1.190	0.480	27.00	1.290	0.300	1.250
	C	50.00	1.260	0.440	10.00	1.215	0.450	1.300

The total reaction cross sections and the grazing angular momenta for the two systems were obtained from the elastic scattering analysis. To test the energy sensitivity of these quantities to the optical model parameters, we have determined for the $^{11}B+^{12}C$ system the total reaction cross sections and grazing angular momenta at various energies using different optical model parameter sets (see Table I). Parameter sets *B* and *C* were extracted from either low energy $^{11}B+^{12}C$ elastic scattering data[14] or from low energy $^{11}B+^{12}C$ total reaction cross section results.[15] These parameter sets gave a poor description of the present high energy (40 and 50 MeV) elastic scattering angular distributions. Consequently, no comparison was made at high energies. Both parameter sets, however, gave an acceptable description of the present 25 MeV elastic scattering angular distribution. As can be seen in Table II, all these optical model parameter sets produce the same energy dependence for the total reaction cross section and grazing angular momentum.

IV. DISCUSSION

Excitation functions of the evaporation residues from the ^{23}Na compound nucleus formed by the $^{11}B+^{12}C$ and the $^{10}B+^{13}C$ entrance channels have been presented in Fig. 4. The total fusion cross sections for the two systems have been presented in Fig. 5. An interesting feature of the data in Fig. 4 is that the excitation functions for the evaporation residues formed using the $^{11}B+^{12}C$ entrance channel are essentially identical in magnitude and energy dependence to the excitation functions for evaporation residues arising from the $^{10}B+^{13}C$ entrance channel. Only two mass groups, 15 and 18, show significant cross-section differences when the two entrance channels are compared.

In an attempt to understand the above results, the available decay channels and the angular momentum brought into the compound nucleus by both systems have been investigated. The grazing angular momentum, extracted from the elastic scattering data, is presented as a function of compound nucleus excitation energy in Fig. 8. Also shown in Fig. 8 is the critical angular momentum of the compound nucleus extracted from the fusion data according to the sharp cutoff model

$$\left[\sigma_f=\pi\lambda^2\sum_{l=0}^{l_{cr}}(2l+1)\right].$$

In Fig. 9, the decay channels available to the compound nucleus are presented. It has been assumed in preparing Fig. 9 that the only decay products which are emitted by the compound nucleus are protons, neutrons, and alpha particles. In support of this assumption are the results of a recent experimental study[16] in this mass and energy region for deuteron emission, the alternative decay channel which might be expected to compete most strongly for entrance channel flux. After studying many entrance channel combinations, these authors found that the ratio of the *pn* to *d* cross section, σ_{pn}/σ_d, could be parametrized in terms of the center-of-mass bombarding energy and the *pn* *Q* value. Applying these results to the present entrance channels, one finds that σ_{pn}/σ_d for the $^{12}C+^{11}B$ ($^{13}C+^{10}B$) is approximately 3 (9) at our lowest energy, and that this ratio increases rapidly with increasing energy for both systems.

TABLE II. Total reaction cross sections and grazing angular momenta for $^{11}B+^{12}C$ obtained from optical model analyses of elastic scattering data. See the text for an explanation of the optical model parameter sets.

		Total reaction cross sections/l grazing		
E_{lab} (MeV)	E_x ^{23}Na (MeV)	Set *A* (mb/$\hbar$)	Set *B* (mb/$\hbar$)	Set *C* (mb/$\hbar$)
15	26.0	665/6.2	675/6.3	634/6.1
20	28.6	943/8.7	955/8.8	919/8.6
25	31.2	1097/10.6	1109/10.8	1077/10.6
30	33.8	1191/12.2	1203/12.4	1175/12.2
35	36.5	1252/13.6		
40	39.1	1295/14.7		
45	41.7	1325/15.8		
50	44.3	1346/16.9		

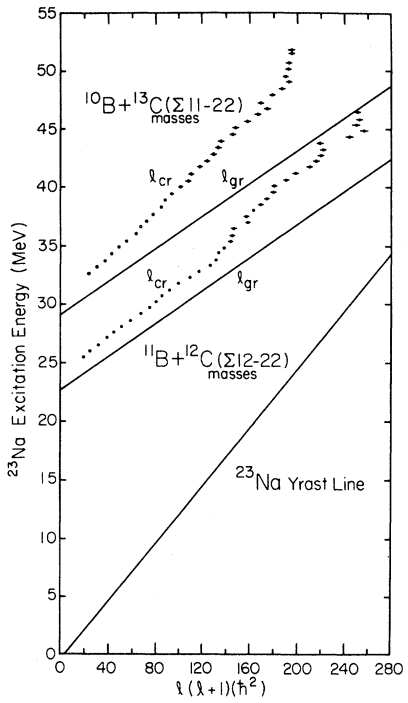

FIG. 8. The critical angular momenta versus ^{23}Na excitation energy. Also shown are a calculated ^{23}Na yrast line and the grazing angular momenta curves for the $^{11}B+^{12}C$ and $^{10}B+^{13}C$ systems.

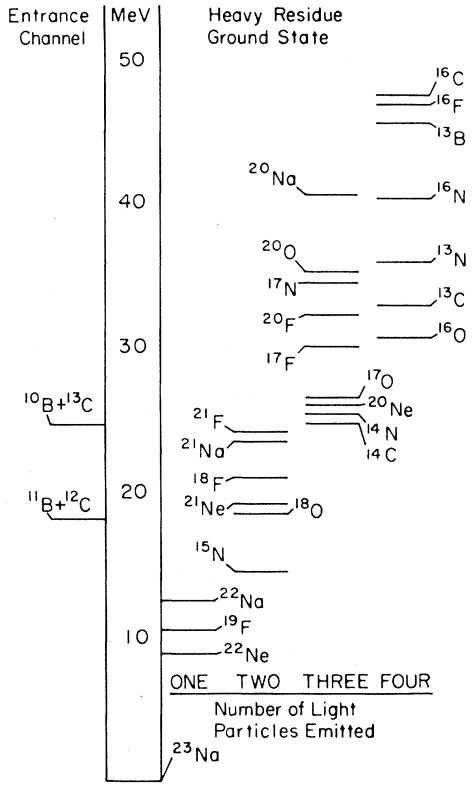

FIG. 9. Ground states of those residual nuclei available for the decay of the ^{23}Na compound nucleus. The residual nuclei have been grouped according to the number of light particles which must be emitted to reach a particular exit channel (assuming neutron, proton, and alpha particle emission only).

As can be seen in Fig. 9, there is a certain threshold energy, corresponding to the positions of the decay channel ground states, associated with the number of light particles emitted. In addition, it is evident that the energy of this threshold increases as the number of emitted light particles increases. To demonstrate that the present data sets exhibit these characteristics, the evaporation residues for the two systems have been presented in Figs. 10 and 11 as a function of the number of light particles emitted. It is immediately apparent that each group corresponding to the emission of a certain number of light particles exhibits a threshold energy below which every mass in that group has either a zero or near zero cross section. As the number of light particles emitted increases, this threshold energy increases.

Once the projectile energy exceeds the threshold for a particular group, the cross sections for all masses in that group increase rapidly. This can be understood in terms of a rapid increase in the level density of each residual nucleus and, consequently, in an increased number of open channels to which the compound nucleus may decay. The cross section for each mass in a group continues to increase until the threshold for the next highest group has been reached. This group then competes for the total entrance channel flux, thus reducing the relative cross sections to those masses in the lower group.

The independence hypothesis for compound nucleus formation and decay[18,19] asserts that when the excitation energy and the angular momentum are specified, the decay process should be entirely determined, independent of the manner in which the compound nucleus was formed. When two entrance channels which lead to the same compound nucleus are compared, therefore, the two systems should exhibit the same decay cross section only if they have the same angular momentum distribution at a particular compound nucleus excitation energy. As can be seen in Fig. 8, the present entrance channels do not share the same angular momentum distribution at the same ^{23}Na excitation energy. At 34 MeV, for example, the $^{11}B+^{12}C$ system can have angular momentum values from 0 to 11 $\hbar$, whereas

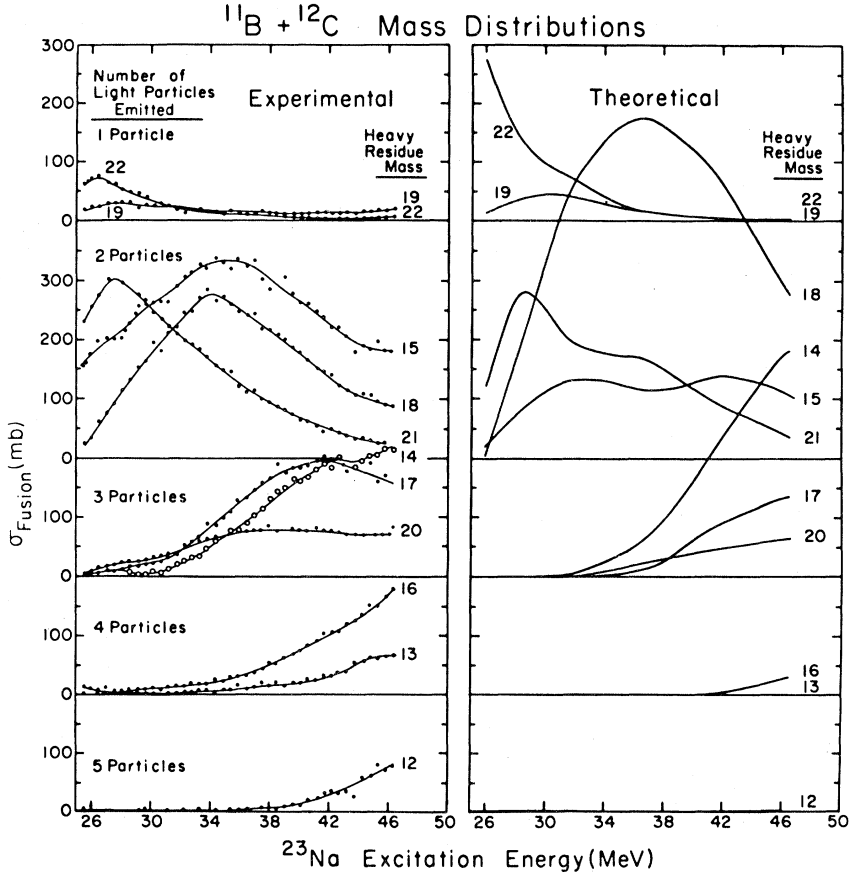

FIG. 10. A comparison between experimental angle-integrated yields for evaporation residues from the $^{11}B + ^{12}C$ system and the Monte Carlo Hauser-Feshbach calculations described in the text.

the angular momentum values for the $^{10}B + ^{13}C$ entrance channel range from 0 to 6$\hbar$. The similar decay cross sections for all masses (except masses 15 and 18) for the two entrance channels suggest that the decay to these exit channels occurs from a compound nucleus formed predominantly by the low entrance channel angular momentum values available to both systems. The large differences in the mass 15 and 18 decay cross sections are presumably due to the large difference in the maximum entrance channel angular momenta for the two systems. In order to demonstrate that the cross section due to the high angular momentum values is indeed substantial, the distribution of the cross section in the sharp cutoff approximation among the allowed l values for the two systems is presented in Table III. While this high angular momentum strength will be shared among all of the energetically available decay channels, it is clear from Fig. 9 that not all decay channels are available. At 34 MeV, the four particle decay channels are energetically closed. Furthermore, while some of the three particle decay channels are open, the energy and, consequently, the angular momentum which can be removed from the compound nucleus by particle decays to these exit channels are small. In addition, since one is at a sufficiently low excitation energy in the residual nuclei, the density of high-spin residual states necessary to remove the high angular momentum of the compound nucleus would not be large. This primarily leaves the one and two particle emission channels to remove most of the high spin flux brought into the compound nucleus by the $^{11}B + ^{12}C$ entrance channel at an excitation energy of 34 MeV. The decay of a high angular momentum compound nucleus state to a residual mass 15, 18, or 19 state is further favored since it involves the emission of alpha particles, decay particles capable of removing larger amounts of angular momentum because of their greater mass. A substantial mass 19 cross sec-

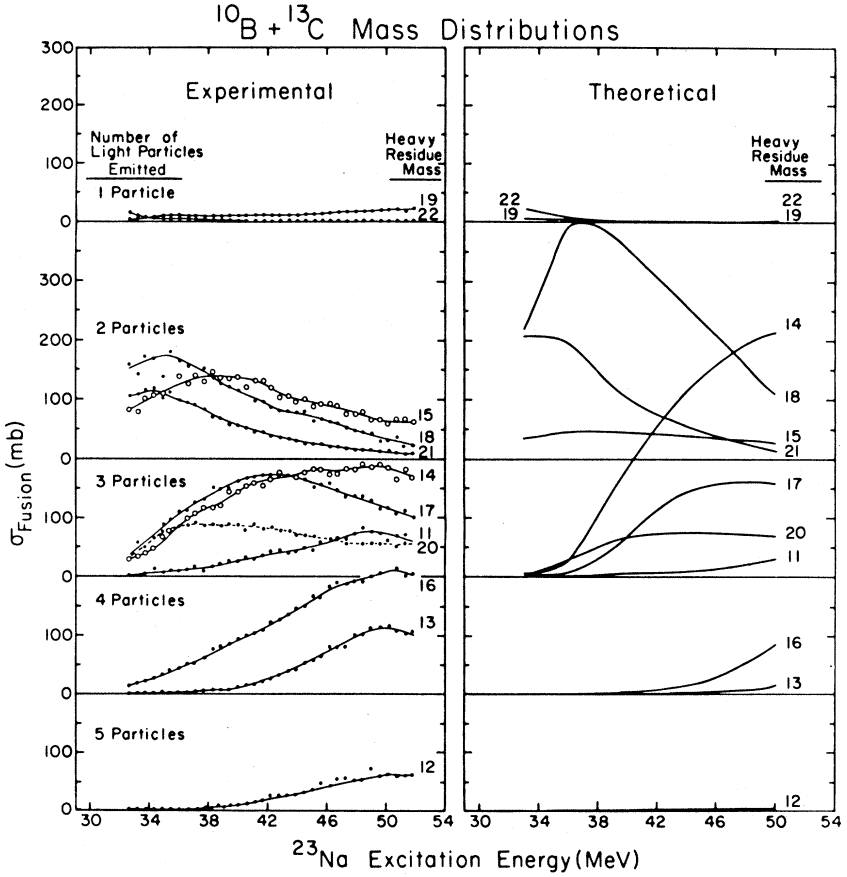

FIG. 11. A comparison between experimental angle-integrated yields for evaporation residues from the $^{10}B+^{13}C$ system and the Monte Carlo Hauser-Feshbach calculations described in the text.

TABLE III. Distribution of cross section among the available l values according to the sharp cutoff model at 34 MeV.

l	σ_{fusion} (mb) $^{11}B+^{12}C$	$^{10}B+^{13}C$
0	6.9	11.8
1	20.7	35.4
2	34.5	59.0
3	48.3	82.6
4	62.2	106.2
5	76.0	129.8
6	89.8	153.4
7	103.6	
8	117.4	
9	131.2	
10	145.0	
11	158.8	
Total	994.4	578.2
Experimental	1014	600

tion is probably not observed, however, because one is well above the ^{19}F particle emission threshold at this energy. A significant part of the high angular momentum flux brought into the compound nucleus by the $^{11}B+^{12}C$ entrance channel and not brought in by the $^{10}B+^{13}C$ entrance channel must appear in the mass 15 and 18 decay channels as experimentally observed. All of the above characteristics of the experimental cross sections for the individual exit channels are qualitatively consistent with the independence hypothesis and the decay of an equilibrated compound nucleus.

Monte Carlo, Hauser-Feshbach calculations, which assumed proton, neutron, and alpha particle emission from the compound nucleus, were performed for both entrance channels with the computer code LILITA.[17] The results of the calculations are presented in Figs. 10 and 11 for the $^{11}B+^{12}C$ and $^{10}B+^{13}C$ systems, respectively. The general procedure adopted in the calculations was to use level density parameters used in previous studies

with no effort made to fit the results of the calculation to the experimental data. While this calculation has done extremely well in predicting the Z distributions of evaporation residues from the $^{12}C+^{14}N$ entrance channel,[10] it has been somewhat less successful in predicting the correct ratio of decay masses for the present systems (see Fig. 12). Precisely what changes (e.g., residual nuclei level densities, distribution of entrance channel angular momenta, etc.) are necessary to bring the calculations into better agreement with the present data has not been investigated at this time.

While the individual decay channels appear to be qualitatively consistent with a simple decay of an equilibrated compound nucleus, the total fusion cross sections suggest a limitation in the formation of the compound nucleus. The clearest evidence of a limitation in the fusion cross section for both systems can be seen in Fig. 8, where the critical and grazing angular momenta for both systems are presented. As the ^{23}Na excitation energy increases, the critical angular momentum line for both systems departs from its respective grazing angular momentum curve, indicating a limitation in the fusion cross section. That this limitation in the total fusion cross section is not due to a critical density of states in the compound nucleus was the subject of a previous paper.[10] There it was pointed out that, while the two systems show evidence for a limitation in their fusion cross sections, the critical angular momentum lines for the two entrance channels do not converge to the same limit at high energies, a condition required if the limitation is produced by a compound nucleus level density (the $^{11}B+^{12}C$ and $^{10}B+^{13}C$ data were shown, for example, to be inconsistent with the compound nucleus model of Lee *et al.*[8]). In view of this fact and the fact that the individual decay channels are consistent with the decay of an equilibrated compound nucleus, one is again led to believe that some feature of the entrance channel is responsible for the fusion cross section limitation. Exactly what feature of the entrance channel nuclei is producing the fusion cross section limitation is not known at this time. While a Glas-Mosel parametrization of these data[21] points to an interesting similarity between these two systems as discussed previously,[10] the meaning of the result is unclear. Additional entrance channel systems need to be studied before a definitive answer to these questions can be obtained.

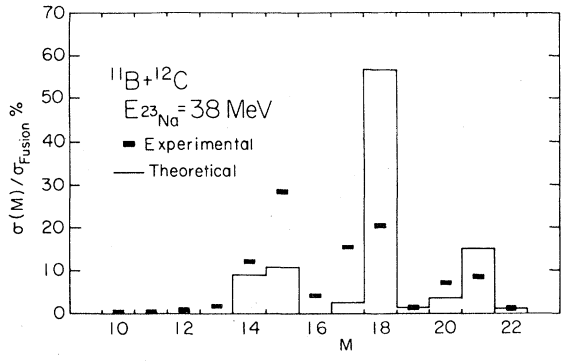

FIG. 12. Angle-integrated yields for evaporation residues with masses from 10 to 22 expressed as a percentage of the $^{11}B+^{12}C$ total fusion cross section. The histograms were obtained from the Monte Carlo Hauser-Feshbach calculations described in the text.

V. SUMMARY

Evaporation residues from the decay of the ^{23}Na compound nucleus formed by the $^{11}B+^{12}C$ and the $^{10}B+^{13}C$ entrance channels have been mass identified with a time-of-flight system. When the evaporation residues for the two entrance channels are compared, the similarities and differences of the decay cross sections to the residual nuclei may be explained qualitatively in terms of the entrance channel angular momentum distributions and the availability of decay channels.

While the individual decay channels are consistent with the decay of an equilibrated compound nucleus, the total fusion cross sections for both entrance channels show evidence of a limitation in the formation of the compound nucleus. As discussed in an earlier paper,[10] this limitation does not appear to be due to a critical density of states in the compound nucleus having been reached. Rather, the total fusion cross section data and the evaporation residue cross sections appear to suggest that some property of the entrance channel nuclei is responsible for the fusion cross section limitations.

ACKNOWLEDGMENTS

The authors would like to thank J. Gomez del Campo for providing the original Hauser-Feshbach calculations and for providing the computer code LILITA. This work was supported in part by the Division of High Energy and Nuclear Physics, U. S. Department of Energy under Contract No. DE-AS05-80ER10714 and by the National Science Foundation.

[1]R. Bass, Phys. Rev. Lett. 39, 265 (1977).
[2]D. Horn and A. J. Ferguson, Phys. Rev. Lett. 41, 1529 (1978).
[3]H. J. Krappe and J. R. Nix, in *Proceedings of the Third International Atomic Energy Symposium on the Physics and Chemistry of Fission, Rochester, 1973* (International Atomic Energy Agency, Vienna, 1974), p. 159.
[4]D. G. Kovar, D. F. Geesaman, T. H. Braid, Y. Eisen, W. Henning, T. R. Ophel, M. Paul, K. E. Rehm, S. J. Sanders, P. Sperr, J. P. Schiffer, S. L. Tabor, S. Vigdor, and B. Zeidman, Phys. Rev. C 20, 1305 (1979), and references therein.
[5]J. Gomez del Campo, R. A. Dayras, J. A. Biggerstaff, D. Shapira, A. H. Snell, P. H. Stelson, and R. G. Stokstad, Phys. Rev. Lett. 43, 26 (1979).
[6]J. P. Wieleczko, S. Harar, M. Comjeaud, and F. Saint-Laurent, Phys. Lett. 93B, 35 (1980).
[7]F. Saint-Laurent, M. Comjeaud, and S. Harar, Nucl. Phys. A327, 517 (1979).
[8]S. M. Lee, T. Matsuse, and A. Arima, Phys. Rev. Lett. 45, 165 (1980).
[9]L. C. Dennis and S. T. Thornton, Phys. Rev. C 22, 340 (1980).
[10]J. F. Mateja, A. D. Frawley, L. C. Dennis, K. Abdo, and K. W. Kemper, Phys. Rev. Lett. 47, 311 (1981).
[11]W. von Oertzen, H. H. Gutbrod, M. Muller, U. Voos, and R. H. Beck, Phys. Lett. 26B, 291 (1968).
[12]F. G. Perey, Phys. Rev. 131, 745 (1963); A. W. Obst, Florida State University Technical Report No. JIB, 1973 (unpublished).
[13]J. F. Mateja, D. P. Stanley, L. V. Theisen, A. D. Frawley, P. L. Pepmiller, L. R. Medsker, and P. B. Nagel, Nucl. Phys. A351, 509 (1981).
[14]W. Bohne, C. K. Gelbke, P. Braun-Munzinger, W. Grochulski, H. L. Harney, and H. Oeschler, Nucl. Phys. A222, 117 (1974).
[15]M. D. High and B. Cujec, Nucl. Phys. A278, 149 (1977).
[16]A. C. Xenoulis, A. E. Aravantinos, C. J. Lister, J. W. Olness, and R. L. Kozub (to be published).
[17]J. Gomez del Campo and R. G. Stokstad, Oak Ridge National Laboratory, Report No. ORNL/TM-7295.
[18]N. Bohr, Nature 137, 344 (1936).
[19]W. Hauser and H. Feshbach, Phys. Rev. 87, 366 (1952).
[20]J. Gomez del Campo, R. G. Stokstad, J. A. Biggerstaff, R. A. Dayras, A. H. Snell, and P. H. Stelson, Phys. Rev. C 19, 2170 (1979).
[21]D. Glas and V. Mosel, Nucl. Phys. A237, 429 (1975).